CHAPTER 2

SYNTHESIS AND CHARACTERIZATION OF PURE ZnO and WO_3-DOPED ZnO

There are 3 parts in this chapter consisting the literature review, flame spray pyrolysis (FSP), synthesis method and characterization of ZnO and WO_3-doped ZnO nanoparticles. In the first part the literature review of ZnO preparation, WO_3 preparation and FSP of ZnO nanoparticles and their composites are presented. In the second part, FSP was employed to produce nanoparticles including the preparation of precursors and chemicals. In the third part, the characterization methods were employed to characterize the nanoparticles properties.

2.1 Literature review

2.1.1 ZnO preparation

ZnO is a versatile material that can be used in many applications. With high demand of this material, there are many techniques for preparing ZnO particles that could be reviewed below.

The synthesis of ZnO nanoparticles using controlled precipitation method was reported by Rodriguez-Paez et al. [1]. Zinc acetate ($Zn(CH_3COO)_2 \cdot 2H_2O$) was used as a precursor. The precipitation process was controlled by potentiometric and conductimetric titration with NH_4OH at room temperature. Two precipitates were formed, the first at pH 7.7 and the second at pH 8.5. Then, resulting precipitates were filtered and redispersed in ethanol several times. During this washing step, zinc alkoxides were nucleated by organic matrix-mediate process. After that, the redispersion of these precipitates was carried out using a high speed turbine and was

dried at 60°C. Finally, the pure ZnO particles were obtained after a thermal treatment in air at 320 °C for 1h was processed.

The synthesis of ZnO particles using acetate-citrate gelation method was reported by Mondelaers et al. [2]. Zinc acetate dehydrate ($Zn(OOCCH_3)_2 \cdot 2H_2O$) and citric acid were used as the precursors. A flow chart of synthesis procedure is shown in Figure 2.1. Study of thermal decomposition of the gel showed that ZnO was formed before the final decomposition step took place. After removing the organic backbone, very small oxide particles were found. The influence of the thermal treatment parameters on the particles size was investigated and a particles growth process was found. By a proper adjustment of the final calcination temperature in the range of 430-870°C in dry air, the mean particle size could be controlled between ~ 11 and 175 nm. It was also seen that even in inert atmosphere, ZnO was formed and that particles morphology was greatly influenced by the calcination atmosphere.

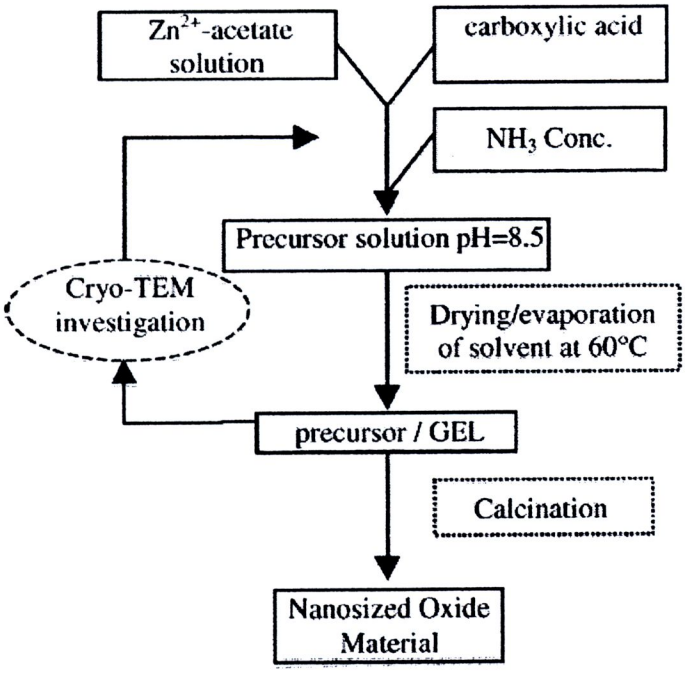

Figure 2.1 Schematic overview of the synthesis of ZnO procedure by acetate-citrate gelation method [2]

The characterization and synthesis of ZnO using template-free method was reported by Wang and Gao [3]. $Zn(NO_3)_2 \cdot 6H_2O$ and $(NH_4)_2CO_3$ were, respectively, dissolved in distilled water to form solution with a certain concentration. $Zn(NO_3)_2$ solution was slowly dropped into the vigorously stirred $(NH_4)_2CO_3$ solution with varying molar ratio of 1:1.25 or 1:2. Then, the precipitate was collected by filtration and repeatedly rinsed with ethanol, then dried at 100 °C for 12h. At last, ZnO nanoparticles were obtained after calcination in the temperature range from 250 to 600°C for 2h. After ZnO particles were characterized with TEM, it was found that these particles had a rod-like morphology

The thermal decomposition process of zinc acetate ($Zn(CH_3COO)_2 \cdot 2H_2O$) using differential thermal analysis (DTA) and thermal gravimetric analysis (TGA) was reported by Zhao et al. [4]. It was found that the water of crystallization was removed at temperature below 200 °C. Anhydrous zinc acetate melted at 210-250 °C, and fully decomposed into ZnO at about 400 °C. The mechanism of decomposition of anhydrous zinc acetate was inferred as a random nucleation mechanism (Avrami equation), and a mechanism model is established as

$$\frac{d\alpha}{dt} = 1.8x10^7 \exp(-103x10^3 / RT)3(1-\alpha)-[-\ln(1-\alpha)]^{2/3} \qquad (2.1)$$

where α is the reacted fraction of initial compound (%) and t is time (second).

Moreover, the synthesis of ZnO particles using spray pyrolysis was studied by Zhao et al. [5]. The solution of zinc acetate dihydrate was sprayed and decomposed at the temperature over 650 °C. It was found that the particle size of ZnO was about 20-30 nm. The product particle morphology and the effect of reaction temperature on the particle properties can be explained by the random nucleation mechanism and model. Furthermore, the synthesis of particles using continuous spray pyrolysis method was

reported by Okuyama and Lenggoro [6]. The particles that were synthesized by this method had many advantages such as adjustable sizes, narrow size distribution, high crystallinity and good stoichiometry. In addition, other materials beside ZnO could also be synthesized by this method.

The synthesis of ZnO particles using the polymerized complex method via an organochemical route was reported by Kwon et al. [7]. A flow chart of synthesis procedure is shown in Figure 2.2. The thermal decomposition and crystallization process were studied by thermogravimetric and differential thermal analysis (TG-DTA), Fourier transform spectroscopy (FT-IR) and X-ray diffraction techniques (XRD). It was found that crystallization of the ZnO particles was detected at 300°C and entirely completed above 400°C.

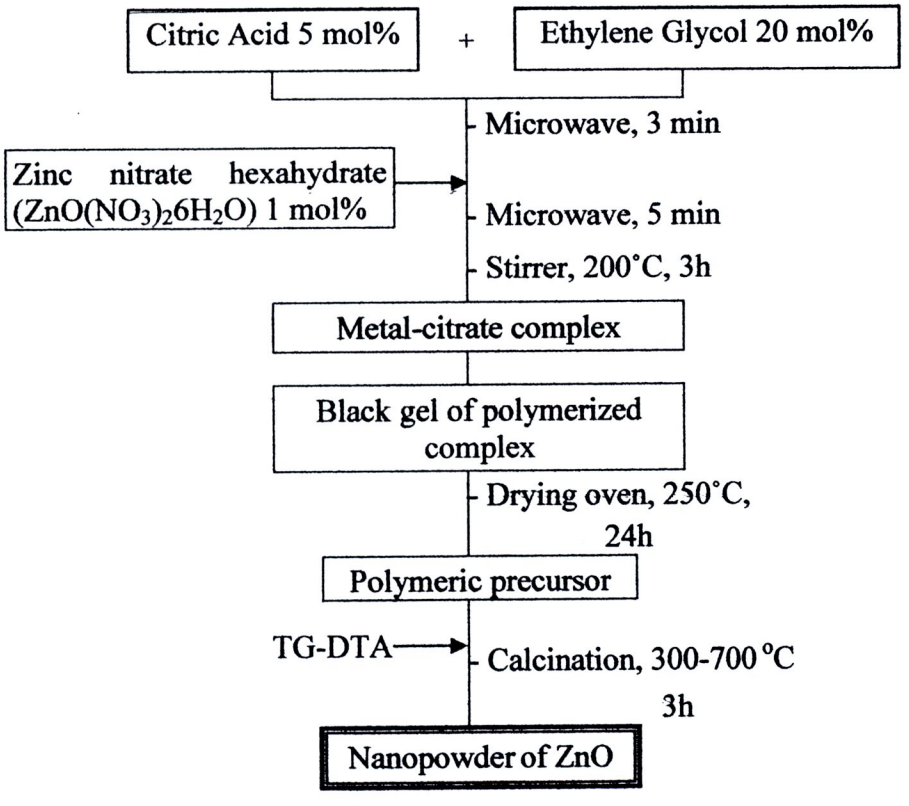

Figure 2.2 Flow chart for synthesis of ZnO nanopowders by the polymerized complex method [7]

A method for the synthesis of ZnO particles using microemulsions system was reported by Singhal et al. [8]. The microemulsion consisted of modified surfactant $Zn(DEHSS)_2$, isooctane as the continuous phase and dry ethanol as the dispersed phase. The precipitation of Zn atom was induced by adding oxalic acid. The microdroplets acted as constrained microreactors for the precipitation reaction. The droplet size as well as the precursor particle size was controlled by the volume of the dispersed phase and the concentration of surfactant in the system. A schematic diagram of microemulsions system is shown in Figure 2.3.

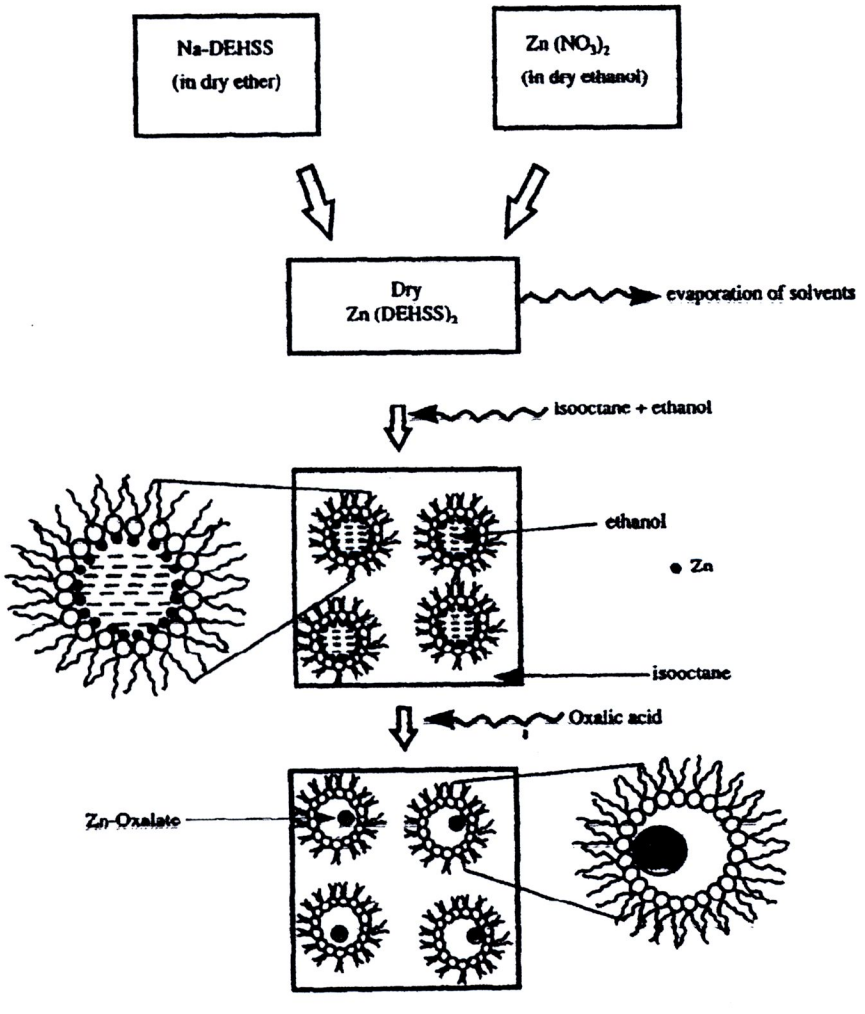

Figure 2.3 Schematic diagram for precipitation of precursor (zinc oxalate) nanoparticles using Zn-AOT/ethanol/isooctane microemulsion system [8]

The synthesis of ZnO nanoparticles by decomposition of the organometallic precursor [$Zn(C_6H_{11})_2$] or homoleptic amido zinc complexes in wet anisole was reported by Rataboul et al. [9]. Firstly, Zn particles were synthesized by decomposition of the organometallic precursor at 130 °C for 30 min. Then, ZnO nanoparticles formed after Zn particles were oxidized at 600 °C for 3h. These nanoparticles were characterized by High resolution electron microscopy (HR-TEM) and X-ray photo-electron spectroscopy (XPS). It was found that the powder consisted of pure hexagonal wurtzite-type phase with a uniform size.

The synthesis of ZnO particles using the precipitation transformation method from $Zn_5(CO_3)_2(OH)_6$ in an aqueous solution was reported by Zhang and Li [10]. The phase transformation process depended on the temperature and amount of NaOH as shown in the equation below.

$$Zn_5(CO_3)_2(OH)_6\,(s) + 4OH^- \rightleftharpoons 5ZnO\,(s) + 2CO_3^{2-} + 5H_2O \qquad (2.2)$$

The flow chart for synthesis of ZnO nanoparticles by the precipitation transformation method is showed in the Figure 2.4.

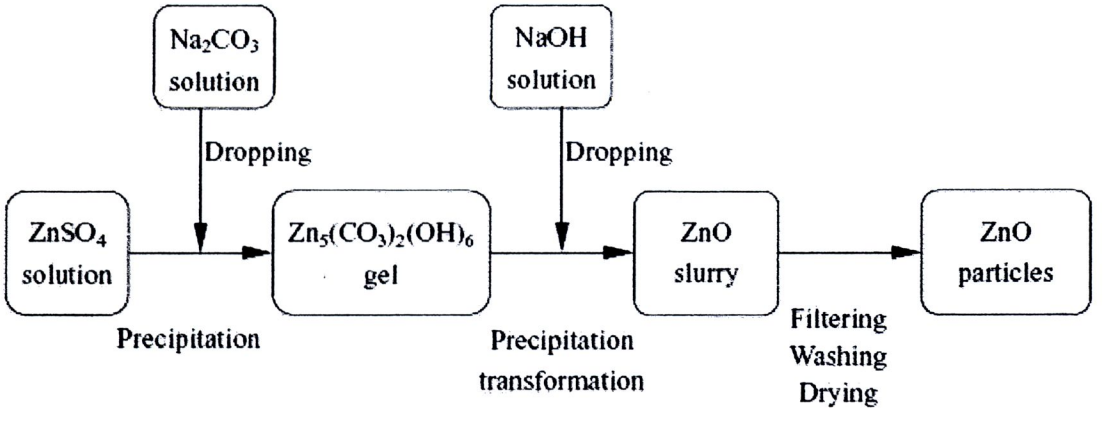

Figure 2.4 Flow chart for synthesis of ZnO nanoparticles by the precipitation transformation method [10]

After the investigation of ZnO particle morphology synthesized by this method, it was found that ZnO crystal is a polar crystal, which belongs to the hexagonal crystal system. The growth habit of a single crystal is pyramid-prism or elongated pyramid-prism. The particle size is in the range of 100 nm.

The synthesis of ZnO particles using the thermal decomposition method using zinc acetate ($Zn(CH_3COO)_2$) coated with β-cyclodextrin (β-CD) as a precursor was reported by Yang et al. [11]. Zinc acetate was chosen as the precursor for its high solubility and low decomposition temperature. $Zn(CH_3COO)_2$ and β-CD were mixed in the water in the molar ratio of 1:2 at room temperature (25 °C) for 120 minutes. Then, the mixture was evaporated by decompressing at 40 °C to remove the water. The resulting solid products were dried in vacuum and ground into powders before use. Then the sample was heat-treated in the muffle at 500 °C for 1h in the air and white-colored ZnO products were obtained. For comparison, pure $Zn(CH_3COO)_2 \cdot H_2O$ was also heat-treated in the same conditions to obtain ZnO powders. The characterization of these samples showed that β-CD could reduce the particle agglomeration and make particles uniform in shape.

2.1.2 WO_3 preparation

WO_3 is one of interesting materials for using in many applications, especially in gas-sensings, electrochromics and photocatalytic applications. There are many methods for preparing WO_3 film and WO_3 particles that could be concluded below.

The preparation of WO_3 thin film using chemical vapor deposition (CVD) technique was reported by Brescacin et al. [12]. $W(CO)_6$ was used as precursors for the comparison. All depositions were performed in a cold-wall reactor using O_2 or N_2/O_2 mixtures as carrier gas. The precursors were sublimated or evaporated from a small crucible. The silicon substrate was placed on a resistively heated suscepetor.

The deposition temperature was fixed at 400 °C. It was found that the best film quality came from the tungsten precursor that had the composition of phosphorus.

The preparation of WO_3 films using an electrodeposition method was reported by Yu et al. [13]. The deposition solution was prepared from Na_2WO_4. The indium-tin-oxide (ITO) coated glass was used as a substrate. The electrical power was pulsed square waves with both "on" and "off" time of 4.0 ms. The peak current density was 1.0 mA/cm^2. Platinum (Pt) foil was used as counter electrode and ITO glass as working electrode. It was found that the deposited films were very smooth and showed good optical properties.

The preparation of pyrochlore WO_3 film using hydrothermal method was reported by Guo et al. [14]. The aqueous sodium tungstate ($Na_2WO_4 \cdot 2H_2O$) solution was used as a precursor. The pH of this precursor was adjusted to be 6.0 by adding hydrochloric acid. The alumina plates coated with a layer of screen-printed gold and ITO glasses were used as substrates. The substrates, on to which the pyrochlore WO_3 films were to be deposited, were immersed in the precursor mixture in a pressure reactor. The reactor was sealed and heated from room temperature to 130 °C, then the temperature was kept at 130 °C for 24h. After that, pyrochlore WO_3 films were characterized by SEM and XRD. It was found that the films were about 50 μm in thickness, had strong mechanical property and good adhesion to the substrates. Moreover, the films showed well-crystallized polycrystals with an octahedral habit.

The preparation of WO_3 films was reported by Cheng et al. [15]. The sol-gel derived tungsten oxide films were deposited from a coating solution via the dip-coating procedure. The solutions were made by dissolving WCl_6 with anhydrous ethanol (C_2H_5OH). The as-deposited film was left in air for 1h to allow the solvent to evaporate and was then fully dried in air at 40 °C. Hydrolysis and condensation of the

film occurred from exposure to ambient moisture during the drying treatments. To obtain powder samples, the coating solution was dried in an open Petri dish in air at 40 °C for several days. From the XRD results, it was found that the as-deposited materials were amorphous while the films heat-treated at 400 °C for 2h crystallize to WO_3.

The preparation of WO_3 films using wet chemical deposition was reported by Kring and Talen [16]. Coating solutions were prepared by dissolving $WOCl_4$ in dry isopropanol. A highly exothermic reaction took place under evolution of HCl. After stirring for a few hours, the solution became colorless. The films were deposited by spin coating. After spin coating, the layers were cured in an oven for 30 min at different temperatures ranging from 80 to 500°C. A final thickness of typically 200 nm was obtained. The structural, electrochemical and electro-optical properties of the films strongly depended on the curing temperature. Crystallization already started around 300°C resulting in a monoclinic phase.

The synthesis of WO_3 nanoparticles using a gas evaporation method for using in NO_2 gas sensing application was reported by Meng et al. [17]. WO_3 nanoparticles were deposited on oxidized silicon substrates by resistive heating of a tungsten filament under an oxygen atmosphere at a low pressure. A schematic diagram of the apparatus used for the formation of WO_3 nanoparticles is shown in Figure 2.5. After the deposition, the WO_3 particles on the substrate were annealed at various temperatures from 400 to 800 °C in air for 1 hour. The obtained nanoparticles are monoclinic WO_3. The average particle size increases with increasing oxygen pressure and with increasing annealing temperature. The sensitivity of the NO_2 sensors made of the WO_3 nanoparticles increases with decreasing particle size.

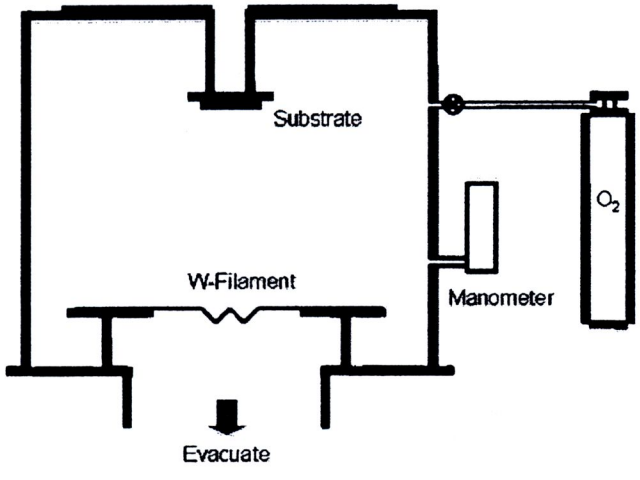

Figure 2.5 Schematic diagram of the apparatus used for the formation of WO_3 nanoparticles [17]

The synthesis of WO_3 nanoparticles using the precipitation method for using in photocatalytic application was reported by Cruz et al. [18]. The ammonium tungstate hydrate ($H_{42}N_{10}O_{42}W_{12-x}H_2O$) was dissolved under continuous stirring distilled water at 80°C. After total dissolution, nitric acid (HNO_3) was added dropwise to the tungstate solution. With a controlled continuous stirring the mixed solution was kept at 80 °C for 40 and 70 min, respectively, in order to check the effect of the time employed in the formation of the WO_3 precursor. After this time, the precipitates were allowed to settle for 1 day at room temperature. The aqueous solution was decanted and distilled water was added with continuous stirring, and then, the sedimentation process of the precipitates was repeated. The precipitates were dried at 80 °C. The obtained precursors were decomposed by thermal treatments at 400, 500 and 600 °C by different time periods in order to follow the formation of WO_3. The resulting samples consisted of nanoparticles with different morphologies and physical properties such as band gap energy and surface area. It was found that the samples

with square-plate morphologies and higher surface areas showed the highest photocatalityc activity in the degradation of indigo carmine in visible light.

2.1.3 Flame spray pyrolysis [19-26]

Many researchers reported that the nanomaterials were synthesized by flame spray pyrolysis technique for decades. The principals and the background concepts of flame spray pyrolysis have been well established and discussed in the chemistry, physics, and engineering fields. The FSP process can be used to produce several materials which widely used in both scientific and commercial communities. Applications are rapidly developed in the medical field, consumer goods, and many areas.

Firstly, the flame-nozzle synthesis of nanoparticles with closely controlled size, morphology, and crystallinity was reported by Wegner et al. [19]. Precise control of the average primary particle size, reduced agglomeration and phase composition was achieved by positioning of the quenching nozzle above the burner and controlling gas and precursor flow rates. Furthermore, the phase composition of the product powders could be controlled also by the burner-nozzle distance. The process had high potential for successful application to other flame configurations and cost-effective synthesis of carbon, silica, alumina and other oxide and non-oxide ceramics with controlled size and limited degree of agglomeration.

The controlled synthesis of nanostructured particles using flame spray pyrolysis was additionally reported by Mädler et al. [20]. The flame spray pyrolysis process was systematically investigated using an external-mixing gas-assisted atomizer supported by six premixed methane/oxygen flamelets. As oxidant air and pure oxygen were used, that served also as droplet dispersion gases. The liquid solvent (fuel), especially its enthalpy content, was an important parameter in FSP as it

affected the total net heating value of the spray flame. The product specific surface area exhibited a maximum and decreased for higher oxidant flow rates. At high flow rates the flame height was reduced substantially as fuel and precursor were oxidized faster in a smaller unit volume accelerating, thus, precursor release at higher temperatures leading to high sintering rates and therefore smaller specific surface area of the product.

The high production rate of nanoparticles produced using flame spray pyrolysis using the silica powder as the representative material was reported by Müller et al. [21]. The effect of powder production rate, dispersion gas flow rate and precursor concentration on product particle size, morphology and carbon content were investigated. The product primary particle size was precisely controlled from 10 to 75 nm and compared to a well-established vapor-fed flame aerosol reactor. The spray flame height increased when increasing the liquid feed rate that corresponded to the production rates using air as dispersion gas. This prolonged the time for fuel combustion resulting in longer flames. The increased feed (or silica production) rate resulted in higher enthalpy content of the flame that leads to longer particle residence times at high temperatures increasing the particle sintering rate resulting in the formation of larger particles. Furthermore, the precursor concentration increased and therefore the silica particle concentration leading to more particle collisions and therefore enhanced growth, which increased the particle diameter especially when complete coalescence took place.

The concept of one-step synthesis of nanoparticles using the liquid-fed aerosol reactor was reported by Mädler et al. [22]. The utilization of liquid-fed reactors for the aerosol-based production of nano-sized powders was reviewed. Aerosol technology was the key process for large-scale production of nano-structured materials. The

understanding of gas-phase synthesis was transferred successfully from classic vapor-fed flames to liquid-fed aerosol reactors, enabling now also the one-step production of demanding and highly functional products. The four main spray methods, namely spray pyrolysis in a tubular reactor (SP), spray pyrolysis using a vapor flame reactor (VFSP), the emulsion combustion method (ECM) and flame spray pyrolysis (FSP), were discussed and the main concepts were compared such as the energy source driving the solvent/fuel evaporation, precursor reaction and final particle formation.

The effect of precursor and oxidant composition in flame synthesis of SiO_2 nanoparticles was reported by Briesen et al. [23]. The effect of precursor source concentration and oxidant composition on the specific surface area of flame-made nanostructured silica particles were investigated in a diffusion flame reactor. This was attributed primarily to the increase of the flame temperature by the additional fuel coming from the organometallic compound. This effect was further pronounced with increasing precursor concentration as it was shown with experiments in a premixed flame reactor. The choice of precursor affected the particle characteristics of silica made in diffusion and premixed flame reactors.

The effect of electrically-assisted falme aerosol synthesis of fumed silica at high production rates was described by Kammler et al. [24]. The control of particle size by external electric fields on flame was investigated during flame synthesis of particles at high production rates. The monotonic increased of specific surface area with field intensity showed that electric fields can be used to precisely control the specific surface area of the product particles. Increasing the precursor concentration led to larger particles. Consequently, the particle size distribution widened as particles experience unequal residence times and sintering temperatures. As a result, electric

fields could not only facilitate the synthesis of ceramic powders with precisely controlled specific surface area, but could also control powder composition.

The role in concepts of aerosol flame reactors for manufacture of TiO_2 nanoparticles as the representive material for studying was given by Stark et al. [25]. Modern flame aerosol synthesis of nanoparticles was a rapidly changing terrain. Advances in process simulation and diagnostics of early particle formation and growth contributed to this development. Classical flame aerosol synthesis was somewhat limited to volatile precursors since the reaction was carried out in a homogeneous gas phase. The concept of flame synthesis could be extended into a heterogeneous system, where the precursor compound was sprayed in the flame. Droplets quickly evaporated and released the compounds into the gas phase. Rapid precursor and solvent evaporation gave products similar to that by classic vapor flame synthesis. For slow evaporation or solvent complexation, even hollow particles could be formed. The reaction and particle formation then proceeded similar than in the flame aerosol synthesis. The extension of classical flame aerosol synthesis to new processes allowed the manufacture of new, high-value products.

The gas-phase synthesis of nanoparticle based on the scale up and design of flame reactor was reported by Wegner et al. [26]. The scale-up and design of flame aerosol reactors were investigated for synthesis of silica and titania nanoparticles. At high fuel-oxidant velocity difference at the burner outlet, the operation of diffusion flame reactors converged to that of premixed ones. Operation of a flame reactor with different fuel composition but with the same combustion enthalpy content still resulted in same size nanoparticles.

2.1.4 Flame-made ZnO nanoparticles and their composites

ZnO nanoparticles synthesized by flame spray pyrolysis technique were reported by many researchers since 2002. The effect of solution feed rate, flame condition, oxidant flow rate, and flame height on particles specific surface area and crystalline size were also discussed as follows.

The homogeneous ZnO nanoparticles that were made using FSP with the precursor of zinc acrylate–methanol–acetic acid solution were reported by Tani et al. [27]. The average primary particle diameter was controlled from 10 to 20 nm by the solution feed rate. Increasing the solution feed rate increased the flame height, and therefore coalescence and/or surface growth was enhanced, resulting in larger primary particles. Compared with ZnO nanoparticles made by other processes, the FSP-made powder exhibited some of the smallest and most homogeneous primary particles.

ZnO nanocrystallites down to 1.5 nm in diameter made using spray combustion of Zn/Si precursors were reported by Mädler et al. [28]. ZnO nanoparticles were smaller than 7 nm in diameter exhibited a so-called quantum size effect. These crystallites exhibited a quantum size effect: blueshift of light absorption with decreasing crystallite size. Stable ZnO quantum dots were made in flames with specifications close to those of wet preparation techniques but at much shorter processing times and without any post-treatment.

The ZnO nanorods made using FSP method were reported by Height et al. [29]. Inorganic nanorods with closely controlled aspect ratio were made by flame spray pyrolysis by a single-step, continuous, and scaleable process. Indium and tin dopants selectively affected a specific ZnO crystal plane and were incorporated into its lattice. Dopant concentrations ranged between 1 and 10 at% with respect to the Zn metal. Nanorod formation was attributed to the higher valency and coordination of

indium and tin dopants relative to zinc and the associated disruption of crystal growth within the Zn plane. In contrast, lithium, with an equivalent ionic radius to these dopants but lower valency than zinc, had no effect on the ZnO texture. The formation of the nanorods within the flame occurred by annealing crystallization during flame cooling. The formation of the nanorods within the flame occurred by annealing crystallization during flame cooling, with the final nanorod aspect ratio determined by dopant concentration.

The high surface area Ag-ZnO catalysts made using FSP were reported by Height et al. [30]. Zinc naphthanate and silver nitrate were used as zinc and silver precursors, respectively. The flame configurations showed that the ZnO primary particle size increased with increasing the liquid precursor feed rates (3/8, 5/5 and 8/3 flames). In each case, silver dopant concentration had no influence on the crystal size of the ZnO. The photocatalytic performance was improved for flame-made materials made at longer high-temperature residence times in the flame.

The synthesis of α-willemite nanoparticles using postcalcination of flame-made ZnO/SiO_2 composites was reported by Tani et al. [31]. A short residence time in the flame could result in the co-existence of the ZnO and SiO_2 clusters without substitution or reaction hindering each other's grain growth. The nano-composite structure of the FSP-made particles could suppress crystalline growth of ZnO during calcination to maintain a high reactivity of ZnO with SiO_2, obtaining pure α-willemite with high specific surface area at low calcinations temperatures. The effects of the Zn/Si ratio on particle properties or ZnO/SiO_2 composite were examined by Tani et al. [32] and compared with those of the pure ZnO and SiO_2 particles made at the same conditions. Polyhedral aggregated of nano-sized primary particles were obtained in all experiments. Powder synthesis was carried out using a spray flame reactor with an

oxygen-assisted nozzle. The composite particles exhibited an excellent thermal stability and little crystalline growth of ZnO. The focus was on the size control and stabilization of ZnO nanoparticles and the effect of precursor Zn/Si ratio on the product particle properties.

The nanoparticles of ZnO, MgO and NiO produced from droplets of aqueous salt solution in the FSP reactor were reported by Seo et al. [33]. Conventional spray pyrolysis, in which electrical furnace reactor was used, was reported to produce nanoparticles only from acetate precursor. The conversion from droplets to particles took place in the diffusion flame which was generated from the combustion of propane and oxygen gases as fuel and oxidizer. Flame spray pyrolysis of aqueous droplets was applied to the synthesis of nanoparticles in order to investigate if the high flame temperature was favorable for the formation of nanoparticles and to find out how the particle morphology changed at the high temperature flame condition.

2.2 Experimental

2.2.1 Chemicals and equipment

The chemicals and equipments that were used for synthesizing pure ZnO and WO_3-doped ZnO by FSP are as follows.

- Zinc naphthenate (Aldrich, 8 wt% Zn, CAS No. 12001-85-3, USA)
- Tungsten (VI)ethoxide (Alfa Aesar, 5% w/v in ethanol, CAS No. 62571-53-3, USA)
- Ethanol (Merck, ≥99.9%, CAS No. 64-17-5, Germany)
- Syringe pump (Inotech, Germany)
- Glass microfiber filters (Whatmann GF/A, 25.7 cm in diameter)
- Vacuum pump (Busch, Seco SV 1040C, Germany)

2.2.2 Precursor preparation for FSP

The volume of 90 mL with concentration of 0.5 mol/L of precursors were prepared for synthesizing the pure ZnO and 0.25, 0.50, 0.75, 1.0, 3.0, 5.0 mol% WO_3-doped ZnO the procedure below.

- Zinc Naphthenate was measured by the volumes that were calculated for synthesizing the pure ZnO, 0.25 mol% WO_3-doped ZnO, 0.50 mol% WO_3-doped ZnO, 0.75 mol% WO_3-doped ZnO, 1.0 mol% WO_3-doped ZnO, 3.0 mol% WO_3-doped ZnO and 5.0 mol% WO_3-doped ZnO as follows: 38.23, 38.14, 38.03, 37.94, 37.85 and 37.08 mL, respectively.
- Tungsten (VI) ethoxide was measured by the volumes that were calculated as the dopants in 0.25-5.0 mol% WO_3-doped ZnO as follows: 1.03, 2.05, 3.06, 4.09, 12.45 and 20.45 mL, respectively.
- Each set of solution between zinc naphthenate and tungsten (VI) ethoxide was dissolved in absolute ethanol to obtain the volume of 90 mL. These precursors had the concentration of 0.5 mol/L.

The amount of chemical for preparing the precursor of FSP could be concluded in Table 2.1 as shown in the next page.

Table 2.1 Precursor preparation for FSP

Flame-made (5/5) 0-5 mol% WO_3-doped ZnO						
Precursor		CAS No.		Density (g/cm^3)		Molar weight (g/mol)
Zinc naphthenate (8 wt% Zn)		12001-85-3		0.962		304.62
Tungsten (VI) ethoxide (5% w/v in ethanol 99.8%)		62571-53-3		-		454.21
Ethanol		64-17-5		0.789		46.07
Elements				Molar weight (g/mol)		
Zn				65.38		
O				15.99		
W				183.84		
ZnO				81.40		
WO_3				231.84		
Samples	Precursor Concentration (mol/L)	Tungsten Ethoxide (mL)	Zinc Naphthenate (mL)	Ethanol (mL)	Total Precusor (mL)	Particles On filter (g) (calculated)
Pure ZnO	0.5	0.0	38.23	51.77	90.0	3.654
0.25 mol% WO_3-doped ZnO	0.5	1.03	38.14	50.90	90.0	3.672
0.50mol% WO_3-doped ZnO	0.5	2.05	38.03	49.91	90.0	3.690
0.75 mol% WO_3-doped ZnO	0.5	3.06	37.94	49.00	90.0	3.708
1.0 mol% WO_3-doped ZnO	0.5	4.09	37.85	48.06	90.0	3.726
3.0 mol% WO_3-doped ZnO	0.5	12.45	37.08	40.66	90.0	3.870
5.0 mol% WO3-doped ZnO	0.5	20.45	36.32	33.25	90.0	3.996

2.2.3 Procedures for synthesizing nanoparticles by FSP

The experimental setup for the synthesis of pure ZnO and WO_3-doped ZnO nanoparticles by FSP was shown in Figure 1.5 (in chapter 1). After the precursors of pure ZnO and WO_3-doped ZnO were prepared, the nanoparticles were synthesized by the procedures as follows:

- The 50 mL of precursor was loaded to glass syringe that was set in the fume hood.
- The capillary tube was inserted in the nozzle. The top of capillary tube was adjusted to be over the nozzle for 1 mm and the bottom was connected to a valve number 1. Then, this valve was connected with valve number 2.
- The glass syringe with precursor was set on syringe pump. This syringe pump was connected to valve number 2 with a tube. Another syringe with solvent was connected to valve number 1.
- The glass fiber filter that has already weighed was set on the top of the collector of flame spray reactor.
- The cooling system was open by turning half a round for thermal exchange reactor and one round for cooling system of nozzle and capillary. The level of cooling system gauge should be 20 for nozzle and lower than 5 for capillary.
- All of the cooling systems were checked for leakage. Then, the syringe with solvent and nozzle were set to connect to a disposal by turning valve number 1.
- The oxygen gas that was used as an oxidant was set as 2.46 L/min and the methane gas was set as 1.19 L/min for igniting the supporting flame.
- The oxygen gas that was used as dispersion gas was set as 4.30 L/min and the oxygen gas that was used as sheet gas was set as 3.92 L/min.

- The syringe with solvent was set to connect to the nozzle for cleaning the capillary tube at the nozzle by turning valve number 1 and the flame color from this solvent was observed. Then, this syringe was changed back to connect to the disposal. After that, another syringe with precursor was connected to the nozzle by setting valve number 2.

- The pressure of the tip of nozzle was set to be 1.5 bar. This value should be stable during the experiment.

- The flow rate of the syringe pump was set as 5 mL per minute. When the flame was stable, the vacuum pump was turned on and the time was counted.

- The liquid precursor mixture was rapidly dispersed by a gas stream and ignited by a premixed methane/oxygen flame. After evaporation and combustion of precursor droplets, particles are formed by nucleation, condensation, coagulation, coalescence as shown in Figure 2.6, and WO_3 deposited on ZnO support as shown in Figure 2.7. Finally, the product nanoparticles were collected on a glass microfiber filters (Whatmann GF/A, 25.7 cm in diameter) with the aid of a vacuum pump (Busch, Seco SV 1040C).

- The height and character of flame were investigated.

- The temperature of heated gas that flowed through the glass fiber filter was kept to be 110 °C for preventing the vapor condensation and the filter burning by controlling the flow rate of cooling water at collector. The highest temperature was recorded.

- The door of fume hood was closed and the goggles were used while this experiment was running.

- The level of precursor had been checked during the experiment. The syringe pump and vacuum pump had turned off before the precursor was used up, at

this time, the flame height decreased quickly. Then, the time of this experiment was recorded.

- The precursor was stopped feeding by setting valve number 2. Then, the nozzle was connected to the syringe that had the solvent for cleaning the whole ignited area by setting valve number 1. After that, the direction of syringe with solvent was changed to disposal by turning valve number 1 for cleaning the residual area.

- The methane gas was turned off. Then, the capillary tube was cleaned by inserting small wire in and out for removing the residual particles. After that, a surgical cotton with alcohol was used for cleaning around the capillary tube.

- All gas valves at mass flow controller and water systems were closed while the goggles were being used. The collector was very hot, we should be careful.

- The screws on the top partition of collector were taken off for moving the glass fiber filter out.

- The parts of flame spray reactor were taken off for cleaning and the collector filter also was cleaned. The goggles and polymer gloves were used during the cleaning.

- All of main valves on the gas tanks were closed. The residual gases at mass flow controller had been vented out before all of gas valves at mass flow controller were closed.

- The glass fiber filters with nanoparticles were weighed.

- The nanoparticles were collected and kept in the fume hood. After that, nanoparticles were sieved and collected in the bottles that had been weighed already. Then, these bottles were weighed again. Finally, the weight data was collected.

The process for generating the pure ZnO and WO_3-doped ZnO nanoparticles were showed in Figure 2.6 and 2.7, respectively. The formation of pure ZnO nanoparticles was processed via nucleation, condensation, coagulation and sintering as shown in Figure 2.6 and for WO_3-doped ZnO nanoparticles, WO_3 nanoparticles were nucleated, condensed and deposited on ZnO support at the last step as shown in Figure 2.7.

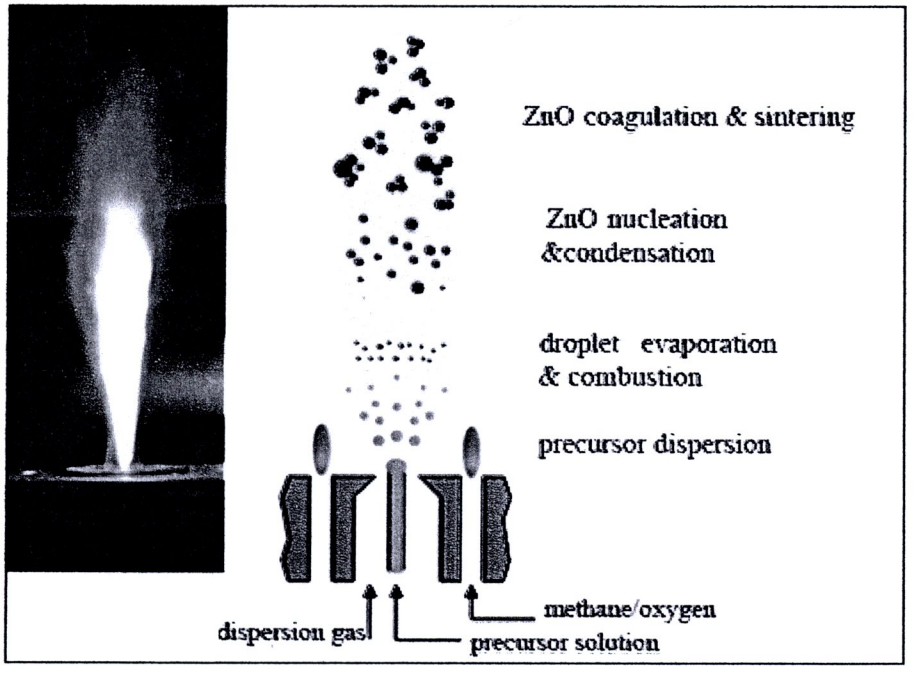

Figure 2.6 Schematic of the FSP unit for pure ZnO production. The liquid precursor was dispersed by a gas stream and ignited by a premixed methane/oxygen flame.

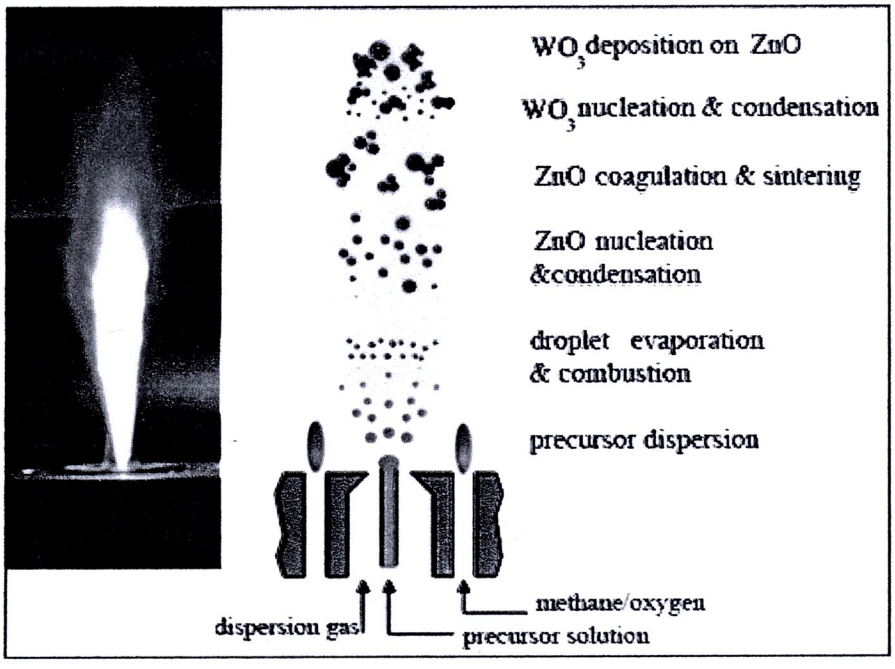

Figure 2.7 Schematic of the FSP unit for WO_3-doped ZnO production. The small WO_3 particles are formed by nucleation, condensation, and deposited on ZnO support at the last step.

2.2.4 Particle characterization

The pure ZnO and WO_3-doped ZnO nanoparticles were characterized by X-ray Diffraction Spectroscopy (XRD), Brunauer-Emmett-Teller (BET) analysis, Scanning Electron Microscopy (SEM), Transmission Electron Microscopy (TEM), Energy Dispersive X-ray Spectroscopy (EDS), UV-Vis absorption spectroscopy and Photoluminescence spectroscopy using the equipment as the following list.

- X-ray diffraction spectrometer (Philip X' Pert PRO PW 3719)
- Brunauer-Emmett-Teller (BET) analysis (Micromeritics Tristar 3000)
- Scanning electron microscope & EDS (JSM-6335F, JEOL)
- Transmission electron microscope (JSM-2010, JEOL)
- UV-Vis absorption spectrophotometer (Varian Cary 50)

- Lab-set photoluminescence spectrometer with excitation wavelength of 273 nm, Wake forest university

2.3 Results and discussion

2.3.1 FSP synthesis

During the synthesis of nanoparticles, all samples showed the yellowish-orange flame appearances as shown in Figure 2.8 (a)-(g) with increasing in the WO_3 concentrations. Moreover, all samples showed the same height of flame of 9.5 cm. These results could be confirmed that WO_3 that was used as a dopant did not affect the flame properties in FSP experiment.

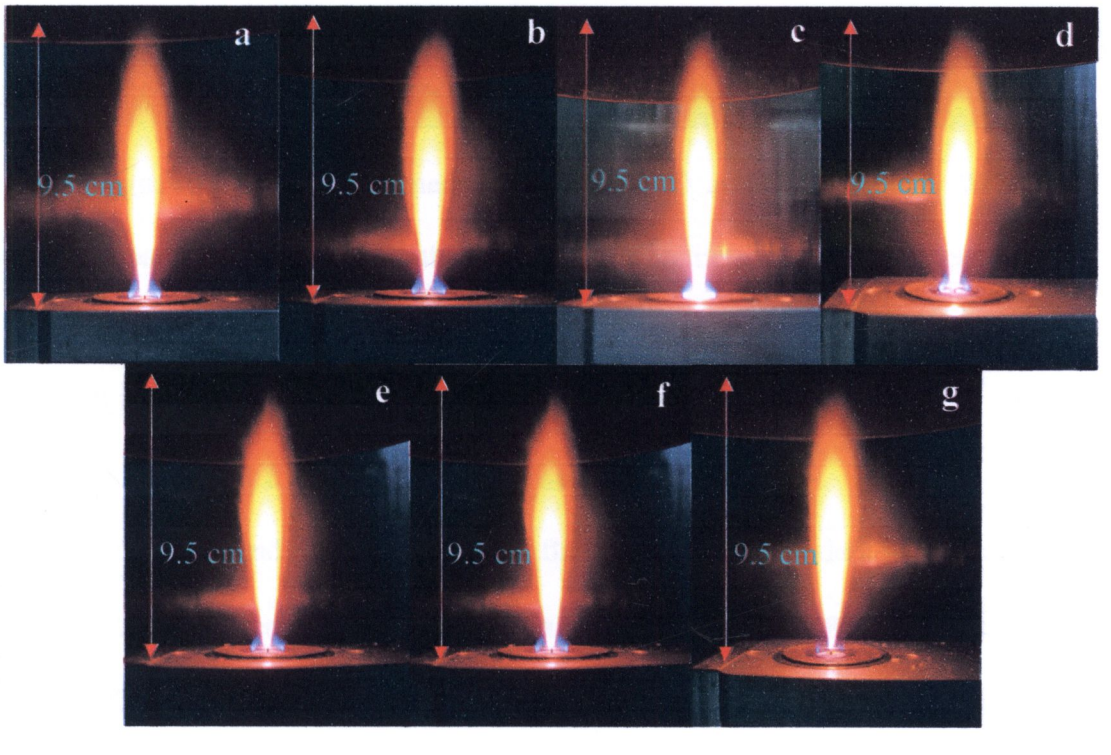

Figure 2.8 Spray flame (0.5 M zinc naphthenate and tungsten (VI) ethoxide in ethanol) of (a) pure ZnO, (b) 0.25 mol% WO_3-doped ZnO, (c) 0.50 mol% WO_3-doped ZnO, (d) 0.75 mol% WO_3-doped ZnO, (e) 1.0 mol% WO_3-doped ZnO, (f) 3.0 mol% WO_3-doped ZnO and (g) 5.0 mol% WO_3-doped ZnO

2.3.2 Powder appearance

Figure 2.9 shows the appearance of pure ZnO and 0.25-5 mol% WO_3-doped ZnO nanoparticles synthesized by FSP. It was found that all samples had the white color that had no difference among them. From this result, it can be concluded that both ZnO and WO_3 had white color and WO_3 did not effect to ZnO appearance.

Figure 2.9 The flame-made (5/5) pure ZnO and 0.25-5 mol% WO_3-doped ZnO nanoparticles ordered from the left to right with increasing WO_3 concentrations.

2.3.3 Characterization of flame-made nanopowders

2.3.3.1 X-Ray diffraction analysis

The phase and crystallinity of the flame-made nanopowders were analyzed by X-ray diffraction spectroscopy using CuKα radiation at $2\theta = 20\text{-}80°$ with a step size of 0.06° and a scanning speed of 0.72°/min. Figure 2.10 shows the XRD patterns of the flame-made (5/5) pure ZnO and WO_3-doped ZnO nanoparticles containing 0.25, 0.50, 0.75, 1.0, 3.0 and 5.0 mol% WO_3. It was found that all samples were highly crystalline, and all peaks can be confirmed to be the hexagonal structure of ZnO, which match well with the JCPDS file No. 89-0510 [34]. Amorphous phase of ZnO and WO_3 peaks

were not found in these patterns. It can be assumed that concentrations of WO_3 were too low and the sizes of WO_3 particles were too small, which affected the WO_3 peaks appearance. The intensity and sharpness of all diffraction patterns were not changed, indicating that the ZnO crystallinity did not change before or after doping with WO_3.

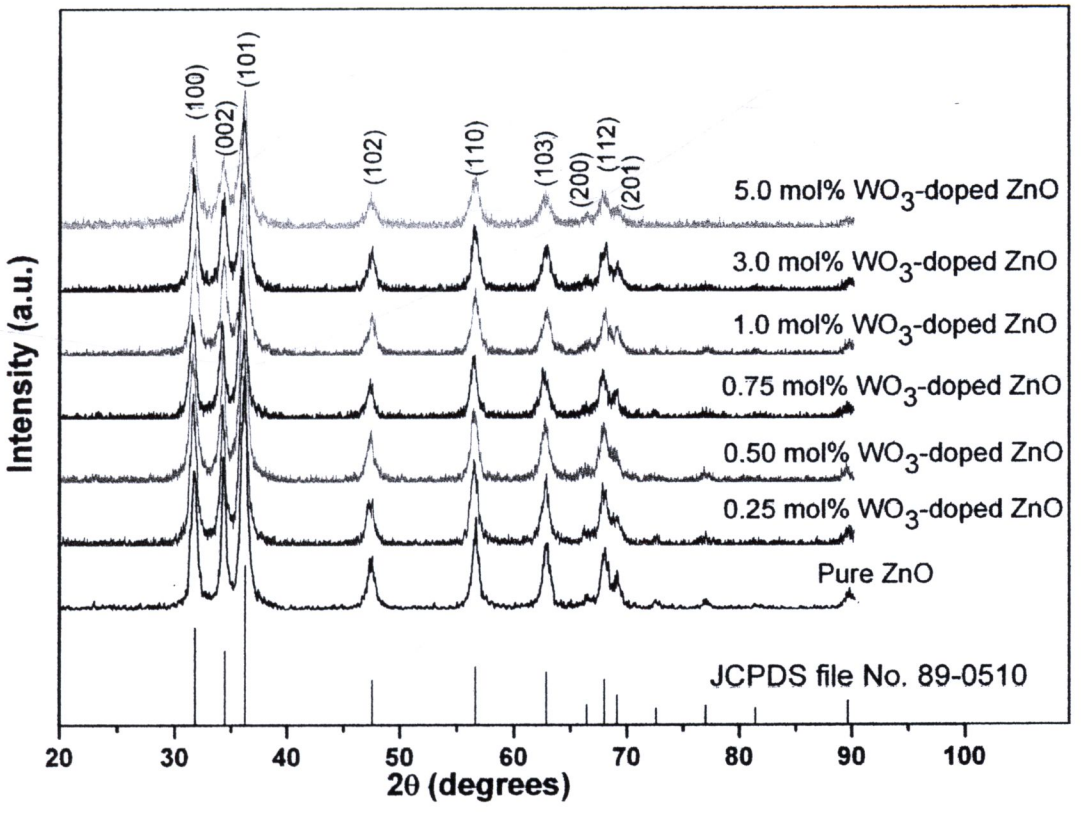

Figure 2.10 XRD patterns of the flame-made (5/5) pure ZnO and WO_3-doped ZnO nanoparticles with different WO_3 concentrations

2.3.3.2 BET analysis

The specific surface area of ZnO samples was measured by nitrogen adsorption at 150 °C, using Brunauer-Emmett-Teller (BET) analysis. The specific surface areas (SSA_{BET}) of pure ZnO and WO_3-doped ZnO nanoparticles containing 0.25, 0.50, 0.75, 1.0, 3.0 and 5.0 mol% WO_3 were 114.2, 104.5, 99.2, 114.6, 121.2,

119.4 and 120.6 respectively. The BET-particle diameter (d_{BET}) can be calculated using the formula as follows:

$$d_{BET} = 6/(\rho_{ZnO} \times SSA_{BET} \times wt\%ZnO + \rho_{WO_3} \times SSA_{BET} \times wt\%WO_3) \quad (2.3)$$

From equation 2.3 [30, 35], d_{BET} is the particle diameter, ρ_{ZnO} and ρ_{WO_3} are the weight density of the ZnO (5.680 g/cm^3 [34]) and WO_3 (7.268 g/cm^3 [36]), respectively. Figure 2.11 shows the comparison of SSA_{BET} and d_{BET} of the pure ZnO and WO_3-doped ZnO nanoparticles with different amount of WO_3. It was found that the calculated particle sizes of all samples were in the same range of 9-10 nm, indicating that the low WO_3 load did not affect the particle size of ZnO.

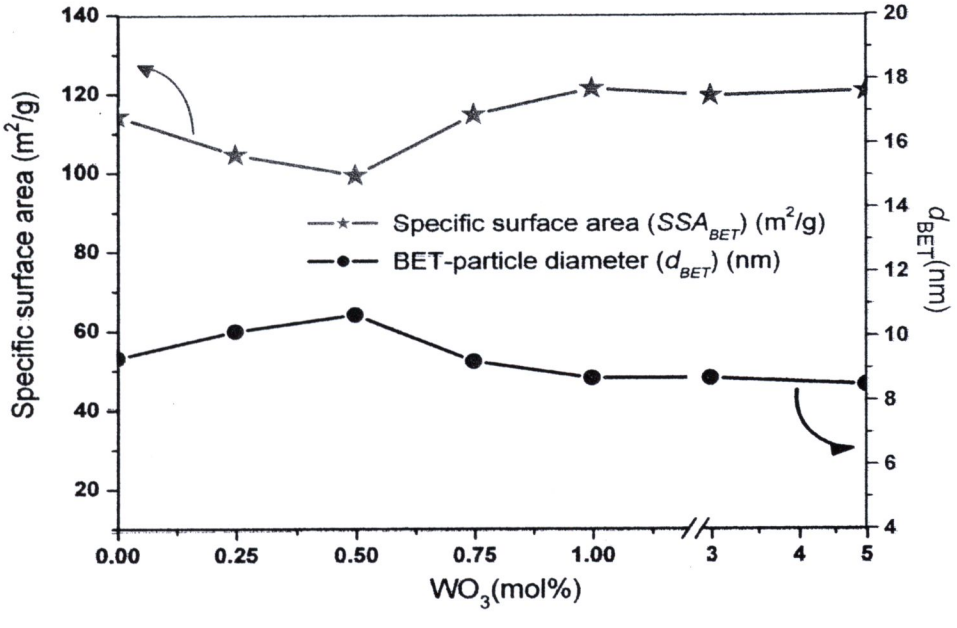

Figure 2.11 The specific surface area (SSA_{BET}) and BET-particle diameter (d_{BET}) of the flame-made (5/5) pure ZnO and WO_3-doped ZnO nanoparticles with different WO_3 concentrations

2.3.3.3 Transmission Electron Microscopy (TEM)

Figure 2.12 shows the TEM bright-field images of flame-made (5/5) (a) pure ZnO, (b) 0.25 mol% WO_3-doped ZnO, (c) 0.50 mol% WO_3-doped ZnO, (d) 0.75 mol% WO_3-doped ZnO, (e) 1.0 mol% WO_3-doped ZnO, (f) 3.0 mol% WO_3-doped ZnO and 5.0 mol% WO_3-doped ZnO nanoparticles. All images could be observed as particles having the clear spherical, hexagonal and rod-like morphologies. The particles sizes were found to be almost in the same range in all figures, which are in good agreement with the BET data. The crystallite sizes of ZnO spherical particles and hexagonal were found to be in the range of 5-25 nm. The ZnO rod-like particles were found to be ranging from 5-10 nm in width and 10-25 nm in length. These particles sizes are consistent with Tani *et al.* [27] and Height *et al.* [29-30]. The diffraction patterns of the particles were shown in the insets. All diffraction patterns illustrated spot patterns of the hexagonal structure of ZnO, indicating that the ZnO nanoparticles are highly crystalline, which are in good agreement with the XRD data. Because the size of WO_3 particles was very small, it could not be observed from TEM modes.

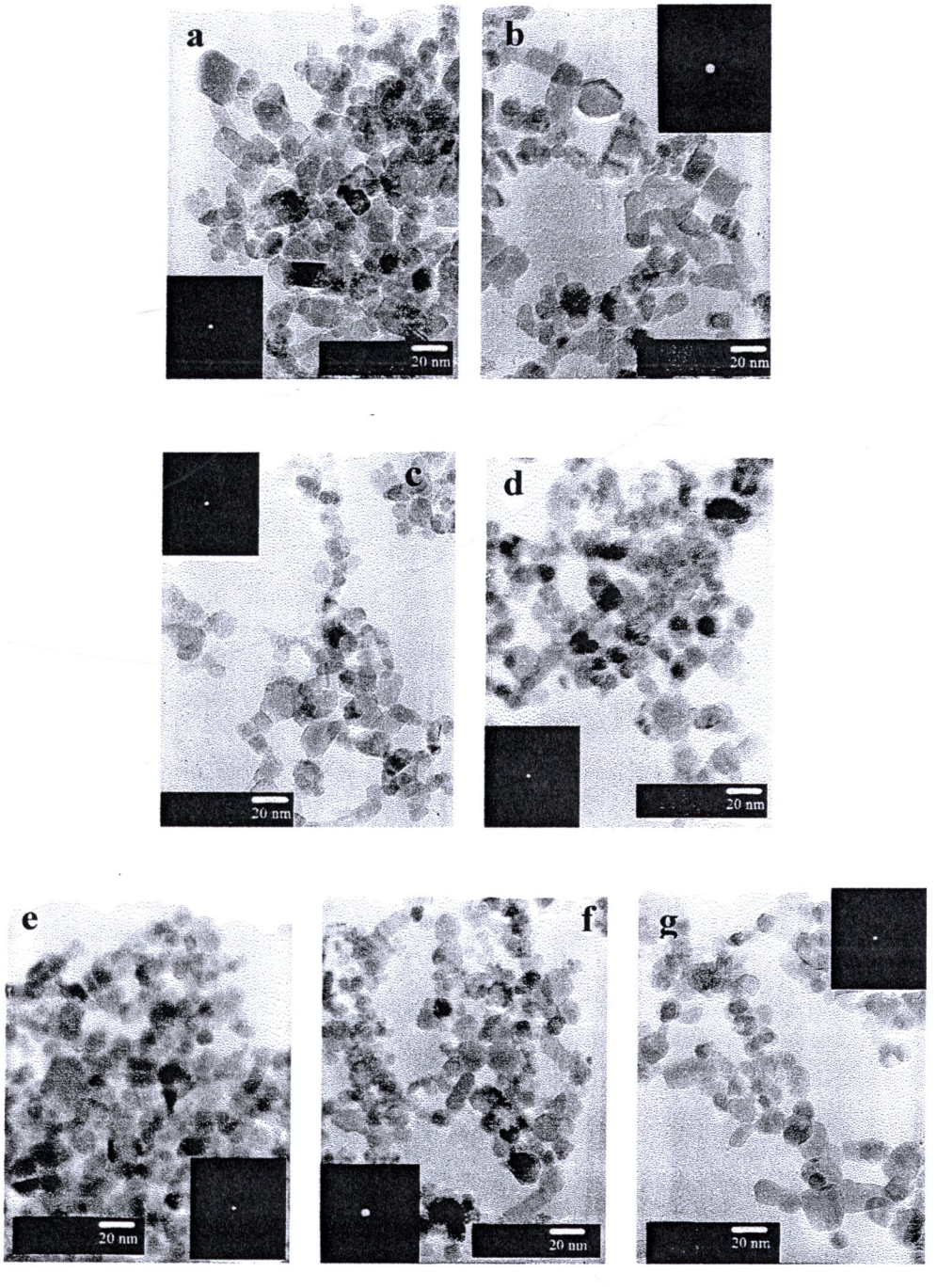

Figure 2.12 TEM bright-field images of the flame-made (5/5) (a) pure ZnO, (b) 0.25 mol% WO_3-doped ZnO, (c) 0.50 mol% WO_3-doped ZnO, (d) 0.75 mol% WO_3-doped ZnO, (e) 1.0 mol% WO_3-doped ZnO, (f) 3.0 mol% WO_3-doped ZnO and 5.0 mol% WO_3-doped ZnO nanoparticles. Insets show the corresponding diffraction patterns of ZnO in each image.

2.3.3.4 Scanning Electron Microscopy (SEM) and Energy Dispersive x-ray Spectroscopy (EDS)

Figure 2.13 shows SEM image of pure ZnO nanoparticles. The EDS spectrum in the inset shows elemental compositions for the region indicated by the white arrow. The Zn and O elements were found in this sample. Figure 2.14, 2.15, 2.16, 2.17, 2.18 and 2.19 show SEM images of 0.25, 0.50, 0.75, 1, 3 and 5 mol% WO_3-doped ZnO nanoparticles, respectively. The corresponding EDS spectra and elemental compositions for the region indicated by the white arrow were shown in the insets. These spectra indicated that the Zn, O and W elements were in these samples. These results confirmed the existence of W in 0.25, 0.50, 0.75, 1, 3 and 5 mol% WO_3-doped ZnO samples that are 0.10, 0.30, 0.29, 0.49, 0.66 and 1.46 at%., respectively. The obtained values are less than the actual values and not in the increasing order due to the chosen and selected area of analysis. The amount of W depending on the selected area of EDS analysis. Moreover, 5 mol% WO_3-doped ZnO nanoparticles had the highest at.% of W, which were corresponding well with dopant concentration.

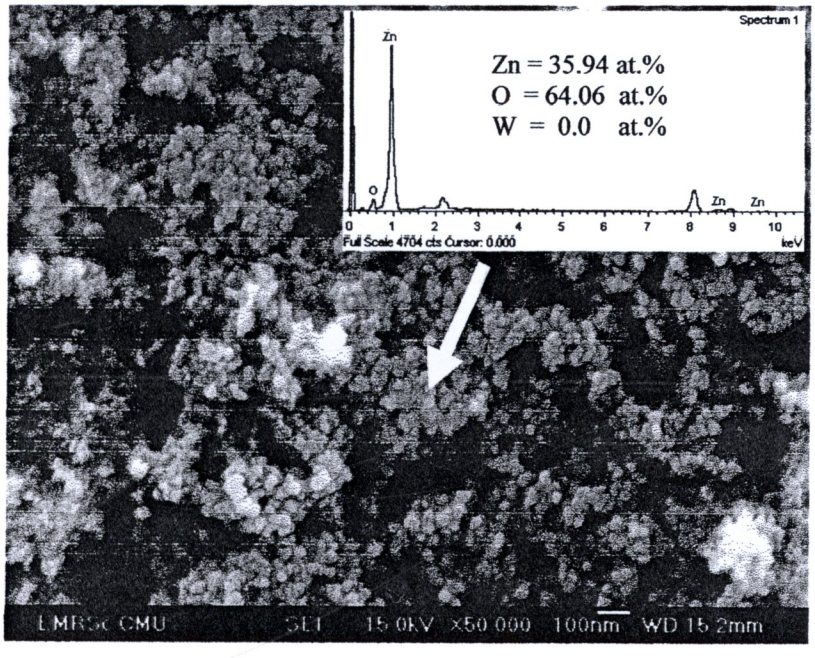

Figure 2.13 SEM image of the flame-made (5/5) pure ZnO nanoparticles. Inset shows EDS spectrum for the region indicated by the white arrow.

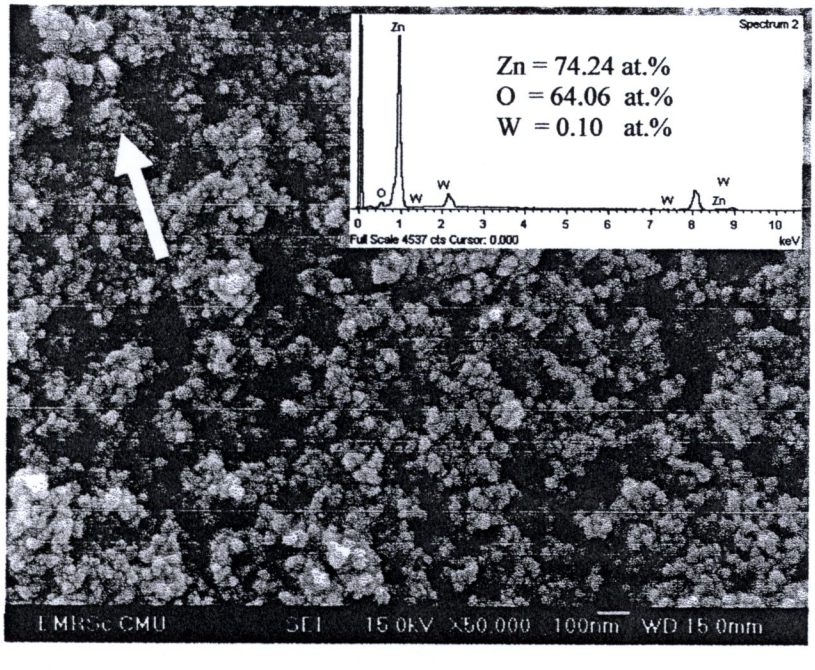

Figure 2.14 SEM image of the flame-made (5/5) 0.25 mol% WO_3-doped ZnO nanoparticles. Inset shows EDS spectrum for the region indicated by the white arrow.

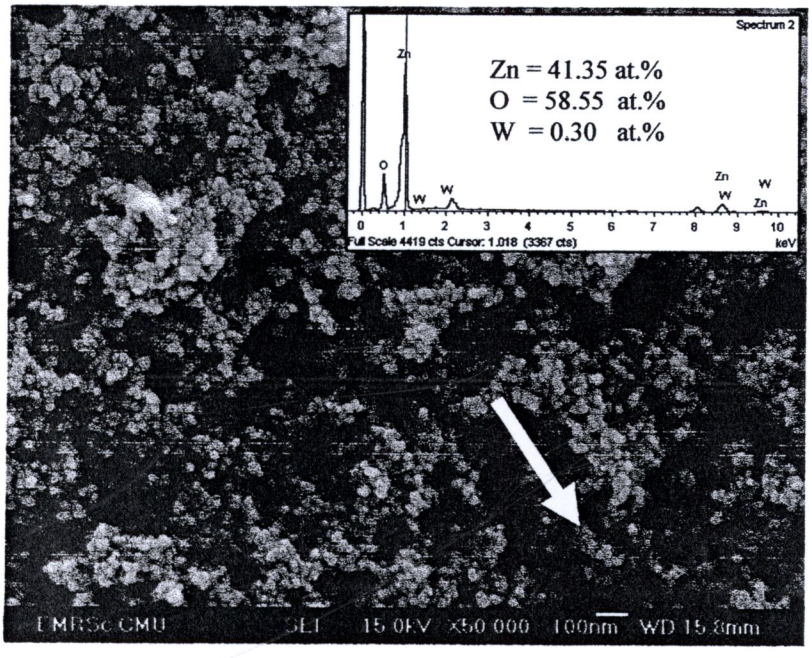

Figure 2.15 SEM image of the flame-made (5/5) 0.50 mol% WO_3-doped ZnO nanoparticles. Inset shows EDS spectrum for the region indicated by the white arrow.

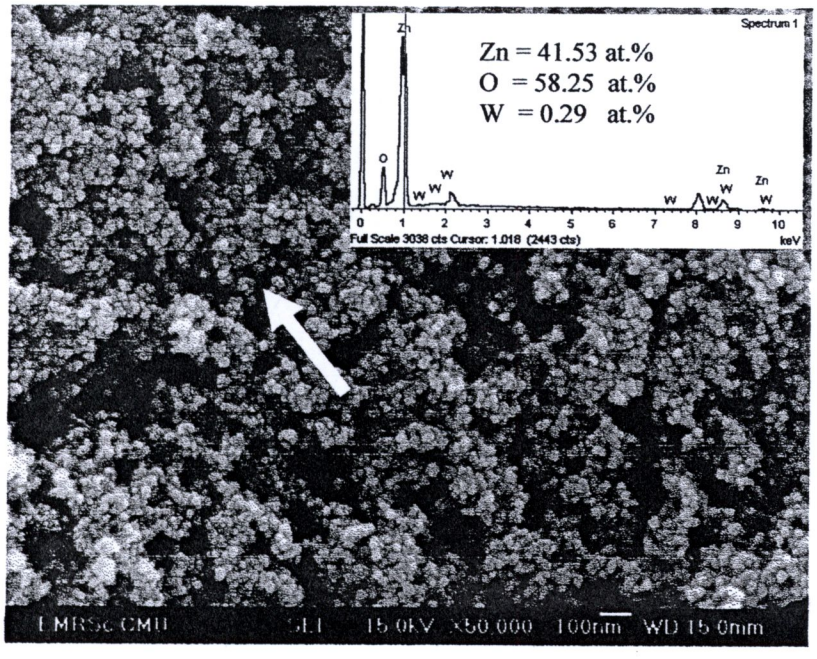

Figure 2.16 SEM image of the flame-made (5/5) 0.75 mol% WO_3-doped ZnO nanoparticles. Inset shows EDS spectrum for the region indicated by the white arrow.

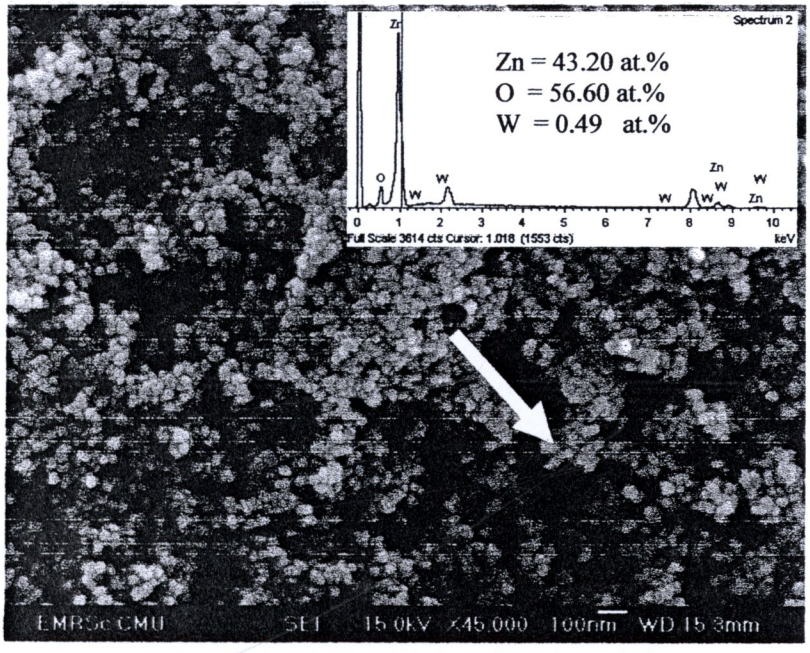

Figure 2.17 SEM image of the flame-made (5/5) 1.0 mol% WO_3-doped ZnO nanoparticles. Inset shows EDS spectrum for the region indicated by the white arrow.

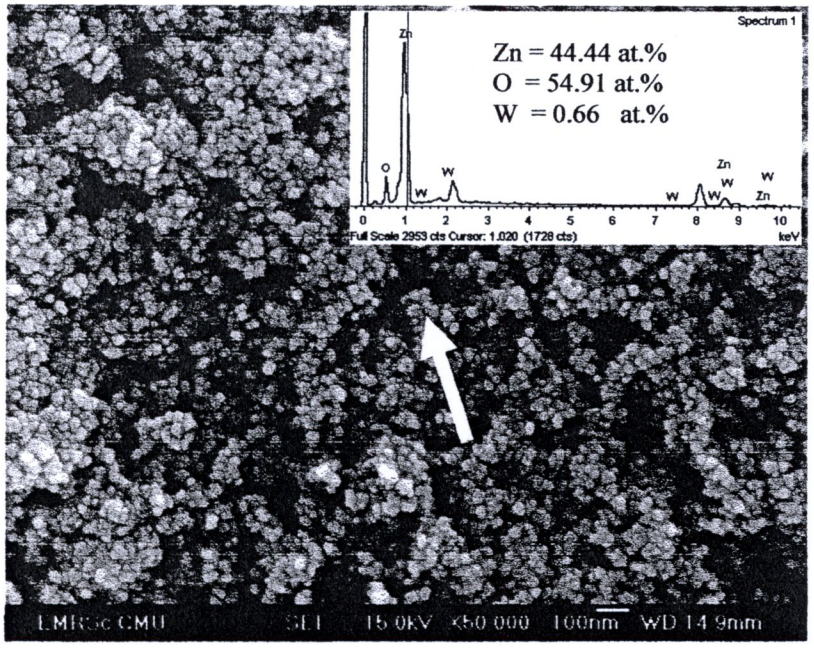

Figure 2.18 SEM image of the flame-made (5/5) 3.0 mol% WO_3-doped ZnO nanoparticles. Inset shows EDS spectrum for the region indicated by the white arrow.

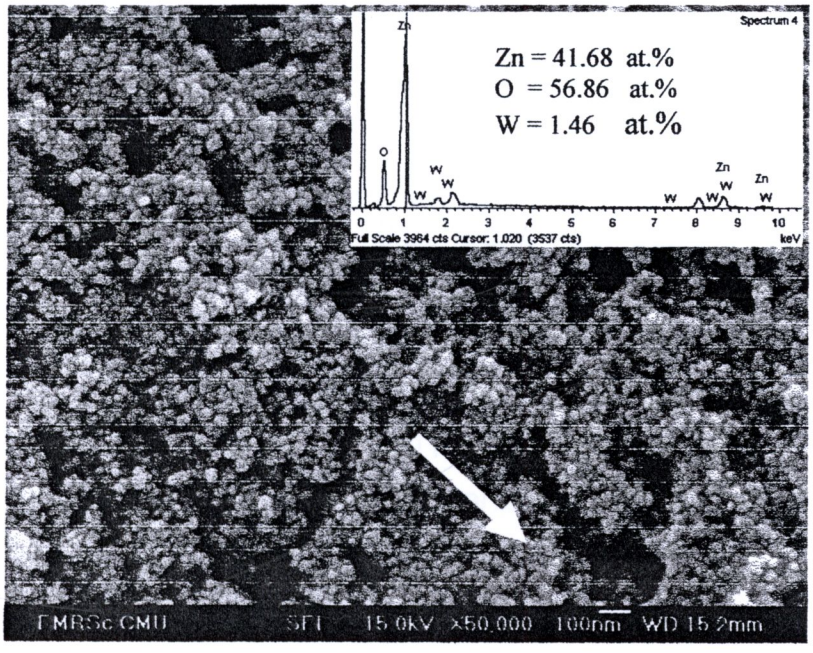

Figure 2.19 SEM image of the flame-made (5/5) 5.0 mol% WO_3-doped ZnO nanoparticles. Inset shows EDS spectrum for the region indicated by the white arrow.

2.3.3.5 UV-Vis absorption spectroscopy

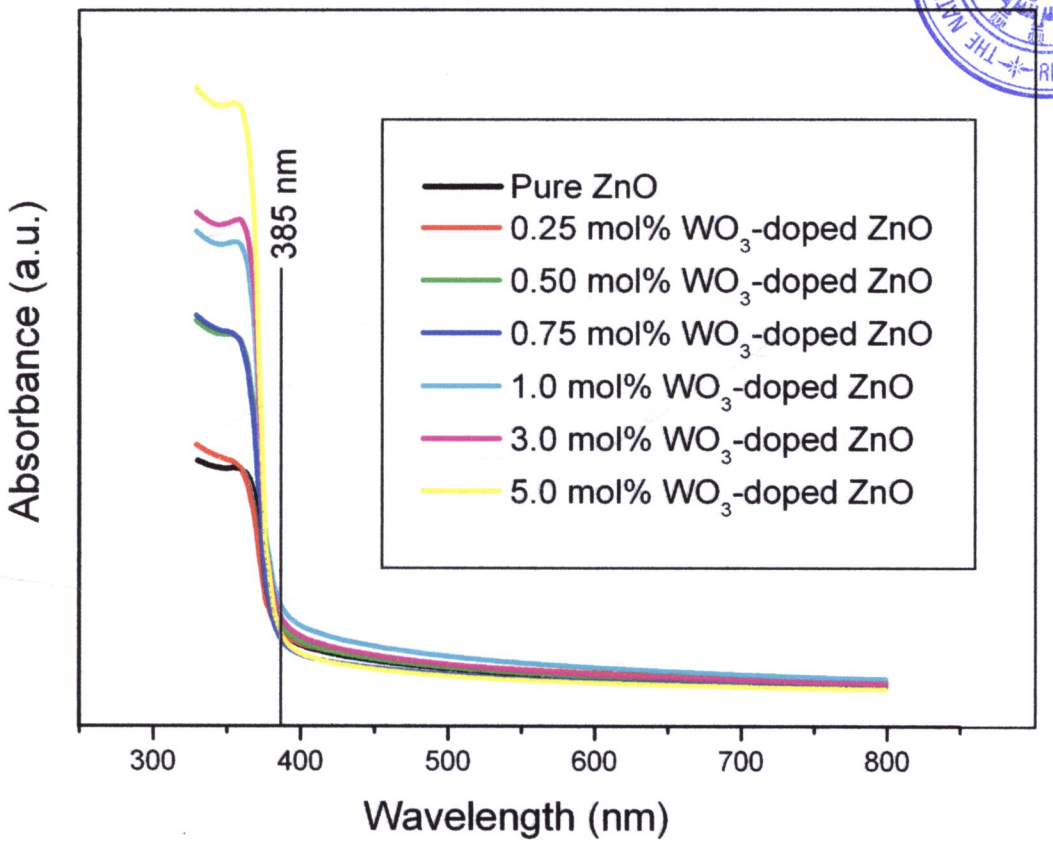

Figure 2.20 Absorption spectra of the flame-made (5/5) pure ZnO and WO_3-doped ZnO nanoparticles with different WO_3 concentrations

Figure 2.20 shows UV-vis spectra of the flame-made (5/5) pure ZnO and WO_3-doped ZnO nanoparticles containing 0.25, 0.50, 0.75, 1.0, 3.0 and 5.0 mol% WO_3. It was found that the absorption spectra of WO_3-doped ZnO nanoparticles with different amount of WO_3 were quite similar to pure ZnO. The absorption edges of all samples were about 385 nm that were ascribed to the fundamental of pure ZnO, which were corresponding to the band-gap of about 3.2 eV [37]. It can be concluded that WO_3 did not affect the ZnO structure. WO_3 must have been deposited onto the ZnO surfaces. The absorption edges of WO_3, about 443 nm (2.8 eV) [37], were not found in these spectra. It was suggested that WO_3 was very small and/or deposited

uniformly on the ZnO surfaces. The concentration of WO_3 on the ZnO surfaces had an effect on the absorption intensity. It was also observed that the absorption intensity of ZnO slightly increased when increased the mixing ratio of the doped WO_3. Such absorption intensity results are in good agreement with those of S. Sakthivel et al. [38].

2.3.3.6 Photoluminescence

Figure 2.21 shows the photoluminescence spectra of the flame-made (5/5) pure ZnO and WO_3-doped ZnO nanoparticles containing 0.25, 0.50, 0.75, 1.0, 3.0 and 5.0 mol% WO_3, using lab-set photoluminescence spectrometer with excitation wavelength of 273 nm at Center for Nanotechnology and Molecular Materials, Wake Forest University. It could notice that all samples have two obvious photoluminescence peaks, the peak at 385 nm should be exhibited from ZnO nanoparticles, which were corresponding to the fundamental band-gap energy of ZnO that was about 3.2 eV [37] and the peak at 412 nm was from the lost energy of exciting laser that scattered from target. Both pure ZnO and WO_3-doped ZnO could show photoluminescence signal with similar curve shape, demonstrating that WO_3 dopant did not give rise to new photoluminescence phenomena. However, the intensities of photoluminescence signals are influenced by this dopant. It could be seen that all photoluminescence signals of WO_3-doped ZnO were higher than that of pure ZnO. The coupling material of two kinds of semiconductors can be produced when a semiconductor is doped with another semiconductor. Thus, the Schottky barrier at the interface between two semiconductors can be formed because of their different Fermi level and electronic band structure. On the basis of the relevant band positions of WO_3 and ZnO, photo-induced electrons easily transfer from ZnO

conduction band to WO_3 conduction band. Hence, photo-induced electrons and holes can be efficiently separated, and the excitonic photoluminescence signals go down. The above discussions demonstrate that the weaker the excitonic photoluminescence spectrum, the higher the separation rate of photo-induced electrons and holes, during WO_3 and ZnO system [39]. Therefore, 0.5 mol% WO_3-doped ZnO nanoparticles show the optimum of photo-induced electrons and holes separation rate among ZnO samples.

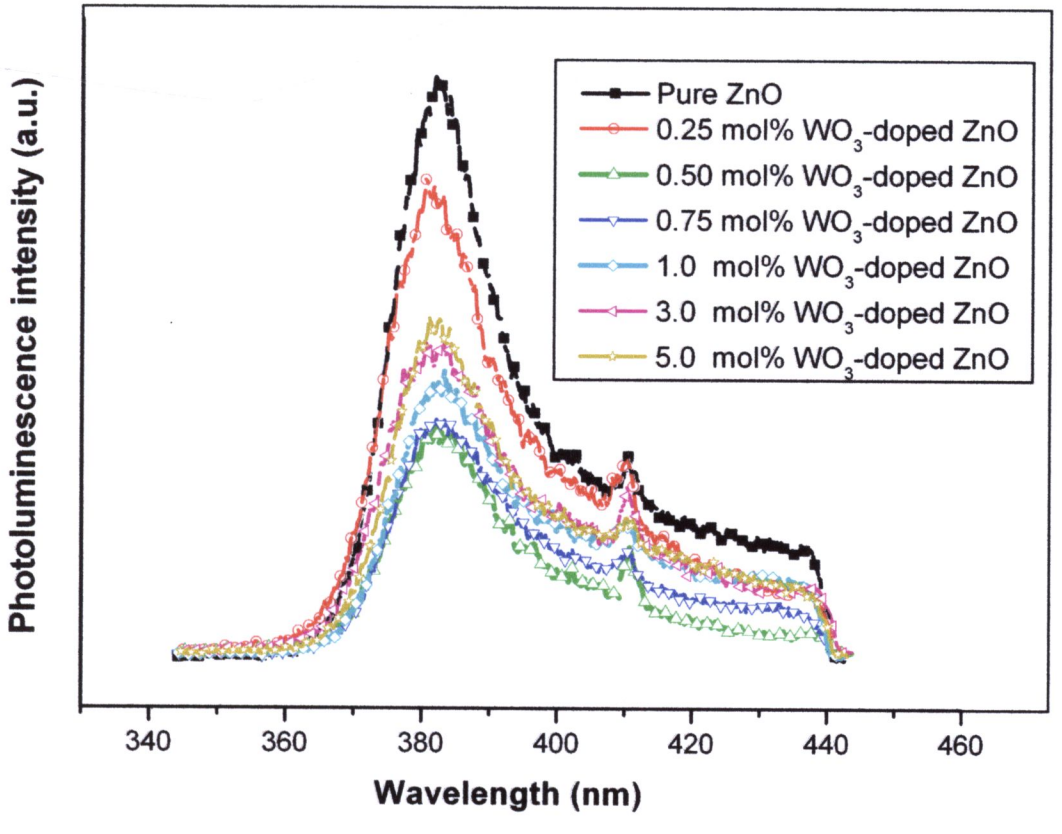

Figure 2.21 Photoluminescence spectra of the flame-made (5/5) pure ZnO and WO_3-doped ZnO nanoparticles with different WO_3 concentrations

2.4 Conclusions

WO_3-doped ZnO nanoparticles containing 0, 0.25, 0.50, 0.75, 1.0, 3.0 and 5.0 mol% of WO_3 were successfully synthesized by FSP from zinc naphthenate and tungsten ethoxide precursors under 5/5 (precursor/oxygen) flame condition. The crystalline phase, morphology and size of undoped ZnO and WO_3-doped ZnO prepared by FSP were observed by XRD, BET, TEM and SEM. The XRD patterns showed that the nanoparticles had the hexagonal phase of ZnO with the JCPDS file No.89-0510. Amorphous phase and WO_3 secondary peaks were not found in these patterns. The TEM image showed nanoparticles having clear spherical, hexagonal and rod-like morphologies. The crystallite sizes of ZnO spherical and hexagonal particles were in the range of 5-20 nm. ZnO nanorods were found to be ranging from 5-10 nm in width and 10-25 nm in length. The W compositions of the ZnO samples were verified by EDS mode. The optical properties of ZnO were characterized by UV-vis absorption spectroscopy and Photoluminescence spectroscopy. The UV-vis absorption edges of all samples were about 385 nm that were ascribed to the fundamental of pure ZnO, which were corresponding to the band-gap energy of about 3.2 eV. Moreover, Photoluminescence spectroscopy showed that the optimum of photo-induced electrons and holes separation rate among ZnO samples was 0.5 mol% WO_3-doped ZnO nanoparticles.

REFERENCES

1. Rodriguez-Paez J.E., Canallero A.C., Villegas M., Moure C., Duran P., Fernanolez J.F. Controlled precipitation methods: formation mechanism of ZnO nanoparticles condensation technique, *J. Eur. Ceram. Soc.,* 2001, **21**, 925-930.

2. Mondelaers D., Vanhoyland G., Van den Rul H., Haen J.D., Van Bael M.K., Mullens J., Van Poucke L.C. Synthesis of ZnO nanopowders via an aqueous acetate-citrate gelation method, *Mater. Res. Bull.*, 2002, **37**, 901-914.

3. Wang J., Gao L. Synthesis and characterization of ZnO nanoparticles assembled in one-dimensional order, *Inorg. Chem. Commun.*, 2003, **6**, 877-881.

4. Yang Y., Li X., Chen J., Chen H., Bao. X., ZnO nanoparticles prepared by thermal decomposition of β-cyclodextrin coated zinc acetate, *Chem. Phys. Lett.*, 2002, **373**, 22-27.

5. Zhao X., Zheng B., Li C., Gu H. Acetate-derived ZnO ultrafine particles synthesizes by spray pyrolysis, *Powder Technol.*, 1998, **100**, 20-23.

6. Okuyama K., Lenggoro I.W. Preparation of nanoparticles via spray route, *Chem. Eng. Sci.*, 2003, **58**, 537-547.

7. Kwon Y.J., Kim K.H., Lim C.S., Shim K.B. Characterization of ZnO nanopowders synthesized by the polymerized complex method via an organochemical route, *J. Ceram. Process. Res.*, 2002, **3**, 146-149.

8. Singhal M., Chhabra V., Kang P., Shah D.O. Synthesis of ZnO nanoparticles for varistor application using Zn-substituted aerosol of microemulsion, *Mater. Res. Bull.*, 1997, **32**, 239-247.

9. Rataboul F., Nayral C., Casanore M-J, Maisonnat A., Chandret B. Synthesis and characterization of monodisperse zinc and zinc oxide nanoparticles from the organometallic precursor $[Zn(C_6H_{11})_2]$, *J. Organomet. Chem.*, 2002, **643-644**, 307-312.

10. Zhang S.C., Li X. G. Preparation of ZnO particles by Precipitation transformation method and its inherent formation mechanisms, *Colloid Surface A.*, 2003, **226**, 35-44.

11. Yang Y., Li X., Chen J., Chen H., Bao X. ZnO nanoparticles prepared by thermal decomposition of β-cyclodextrin coated zinc acetate, *Chem. Phys. Lett.*, 2002, **373**, 22-27.

12. Brescacin E., Basato M., Tondello E. Amorphous WO_3 Films via Chemical Vapor Deposition from Metallorganic Precursors Containing Phosphorus Dopant, *Chem. Mater.*, 1999, **11**, 314–323.

13. Yu Z.R., Jia X.D., Du J.H., Zhang J.Y. Electrochromic WO_3 films prepared by a new electrodeposition method, *Sol. Energ. Mat. Sol. C.*, 2000, **64**, 55–63.

14. Guo J.D., Li Y.J.J., Whittingham M.S. Hydrothermal synthesis of electrode materials Pyrochlore tungsten trioxide film, *J. Power Sources*, 1995, **54**, 461–464.

15. Cheng W., Baudrin E., Dunn B., Zink J.L. Synthesis and electrochromic properties of mesoporous tungsten oxide, *J. Mater. Chem.*, 2001, **11**, 92–97.

16. Krings L.H.M., Talen W. Wet chemical preparation and characterization of electrochromic WO_3, *Sol. Energ. Mat. Sol. C.*, 1998, **54**, 27–37.

17. Meng D., Yamazaki T., Shen Y., Lui Z., Kikuta T. Preparation of WO_3 nanoparticles and application to NO_2 sensor, *Appl. Surf. Sci.*, 2009, **256**, 1050-1053.

18. Cruz A.M., Martinez D.S., Cuellar E.L. Synthesis and characterization of WO_3 nanoparticles prepared by the precipitation method: Evaluation of photocatalytic activity under vis-irradiation, *Solid State Sci.*, 2009, **12**, 1-7.

19. Wegner K., Stark W.J., Pratsinis S.E. Flame-nozzle synthesis of nanoparticles with closely controlled size, morphology and crystallinity, *Mater. Lett.*, 2002, **55**, 318-321.

20. Mädler L., Kammler H.K., Mueller R., Pratsinis S.E. Controlled synthesis of nanostructured particles by flame spray pyrolysis, *J. Aerosol Sci.* 2002, **33**, 369-389.

21. Müller R., Mädler L., Pratsinis S.E. Nanoparticle synthesis at high production rates by flame spray pyrolysis, *Chem. Eng. Sci.* 2003, **58**, 1969-1976.

22. Mädler L. Liquid-fed aerosol reactors for one-step synthesis of nano-structured particles. *KONA*, 2004, **22**, 107-120.

23. Briesen H., Fuhrmann A., Pratsinis S.E. The effect of precursor in flame synthesis of SiO2, *Chem. Eng. Sci.*, 1998, **55**, 4105-4112.

24. Kammler H.K., Pratsinis S.E. Electrically-assisted flame aerosol synthesis of fumed silica at high production rates, *Chem. Eng. Process.*, 2000, **39**, 219-227.

25. Stark W.J., Pratsinis S.E. Aerosol flame reactors for manufacture of nanoparticles, *Powder Technol.*, 2002, **126**, 103-108.

26. Wegner K., Pratsinis S.E. Gas-phase synthesis of nanoparticles: scale-up and design of flame reactors, *Powder Technol.*, 2005, **150**, 117-122.

27. Tani T., Mädler L., Pratsinis S.E. Homogeneous ZnO nanoparticles by flame spray pyrolysis, *J. Nanopart. Res.*, 2002, **4**, 337-343.

28. Mädler L., Stark W.J., Pratsinis, S.E. Rapid synthesis of stable ZnO quantum dots, *J. Appl. Phys.*, 2002; 92: 6537-6540.

29. Height M.J., Mädler L., Krumeich F., Pratsinis S.E. Nanorods of ZnO made by flame spray pyrolysis, *Chem. Mater.*, 2006, **18**, 572-578.

30. Height M.J., Pratsinis S.E., Mekasuwandumrong O., Praserthdam P. Ag-ZnO catalysts for UV-photodegradation of methylene blue, *Appl. Catal., B-Environ.*, 2005, **63**, 305-312.

31. Tani T., Mädler L., Pratsinis S.E. Synthesis of α-willemite nanoparticles by post-calcination of flame-made ZnO/SiO2 composites, *Part. Part. Syst. Char.*, 2002, **19**, 354-358.

32. Tani T., Mädler L., Pratsinis S.E. Synthesis of zince oxide/silica composite nanoparticles by flame spray pyrolysis, *J. Mater. Sci.*, 2002, **37**, 4627-4632.

33. Seo D.J., Park S.B., Kang Y.C., Choy K.L. Formation of ZnO, MgO and NiO nanoparticles from aqueous droplets in flame reactor. *J. Nanopart. Res.*, 2003, **5**, 199-210.

34. Sawada H., Wang R., Sleight A.W. An Electron Density Residual Study of Zinc Oxide, *J. Solid State Chem.*, 1996, **122**, 148-150.

35. Teoh W.Y., Mädler L., Beydoun D., Pratsinis S.E., Amal R., Direct (one-step) synthesis of TiO_2 and Pt/TiO_2 nanoparticles for photocatalytic mineralisation of sucrose, *Chem. Eng. Sci.*, 2005, **60**, 5852-5861.

36. Aird A., Domeneghetti M.C., Mazzi F., Tazzoli V., Salje E.K.H. Sheet superconductivity in WO_{3-x}: crystal structure of the tetragonal matrix, *J. Phys.-Condens. Matter.*, 1998, **10**, L569-L574.

37. Li D., Haneda H. Photocatalysis of sprayed nitrogen-containing Fe_2O_3–ZnO and WO_3–ZnO composite powders in gas-phase acetaldehyde decomposition, *J. Photoch. Photobiol. A*, 2003, **160**, 203-212.

38. Sakthivel S., Geissen S.U., Bahnemann D.W., Murugesan V., Vogelpohl A. Enhancement of photocatalytic activity by semiconductor heterojunctions: α-Fe_2O_3, WO_3 and CdS deposited on ZnO, *J. Photoch. Photobiol. A*, 2002, **148**, 283-293.

39. Liqiang J., Yichun Q., Baiqi W., Shudan L., Baojiang J., Libin Y., Wei F., Honggang F., Jiazhong S. Review of photoluminescence performance of nano-sized semiconductor materials and its relationships with photocatalytic activity, *Sol. Energ. Mat. Sol. C.*, 2006, **90**, 1773-1787.